Topology Evolution and Gelation Mechanism of Agarose Gel

Jun-Ying Xiong,[†] Janaky Narayanan,[‡] Xiang-Yang Liu,*[,‡] Tan Kok Chong,[§] Shing Bor Chen,[†] and Tai-Shung Chung[†]

Department of Chemical and Biomolecular Engineering, National University of Singapore, 10 Kent Ridge Crescent, Singapore 119260, Singapore, Department of Physics, National University of Singapore, 2 Science Drive 3, Singapore 117542, Singapore, and Hwa Chong Junior College, Singapore, Singapore

Received: December 5, 2004; In Final Form: January 31, 2005

Kinetics as well as the evolution of the agarose gel topology is discussed, and the agarose gelation mechanism is identified. Aqueous high melting (HM) agarose solution (0.5% w/v) is used as the model system. It is found that the gelation process can be clearly divided into three stages: induction stage, gelation stage, and pseudoequilibrium stage. The induction stage of the gelation mechanism is identified using an advanced rheological expansion system (ARES, Rheometric Scientific). When a quench rate as large as 30 deg C/min is applied, gelation seems to occur through a nucleation and growth mechanism with a well-defined induction time (time required for the formation of the critical nuclei which enable further growth). The relationship between the induction time and the driving force which is determined by the final setting temperature follows the 3D nucleation model. A schematic representation of the three stages of the gelation mechanism is given based on turbidity and rheological measurements. Aggregation of agarose chains is promoted in the polymer-rich phase and this effect is evident from the increasing mass/length ratio of the fiber bundles upon gelation. Continuously increasing pore size during gelation may be attributed to the coagulation of the local polymer-rich phase in order to achieve the global minimum of the free energy of the gelling system. The gel pore size determined using turbidity measurements has been verified by electrophoretic mobility measurements.

Introduction

Supramolecular order of biological significance found in hydrogels[1] formed by biopolymers is of interest from both theoretical and practical aspects. Sol−gel transition and gel topology involve many conceptual aspects, such as phase transition and scaling, and therefore are of high intrinsic interest. In the practical aspects, these hydrogels attract considerable attention due to their gelling properties which find numerous applications in different fields, such as chromatography and filtration, photography, hematology, food technology, and pharmacy.

Agarose, which is a repetitive, essentially uncharged, marine polysaccharide (Figure 1), is often used as the model biopolymer in gelation. Since complications due to electrostatic interactions and additional molecular species are absent in aqueous agarose systems, they are quite suitable for researchers to study the nature of the gelation of biopolymers. Although agarose gels have been extensively studied in the past 30 years, the gelation mechanism still remains elusive. Many researchers[3−5] use laser light scattering to study agarose gelation. Using Cahn's theory[6] they determine whether a spinodal decomposition process occurs or not. However, conclusions from different researchers seem somewhat inconsistent with each other. We discuss some of these issues in the Results and Discussion section of this paper. Furthermore, as pointed out by Guenet,[7] the laser scattering technique alone need not necessarily support the spinodal process. Despite the fact that much effort has been devoted to understand the agarose sol−gel transition,[3−5,7,8] studies on the evolution of agarose gel topology upon gelation are rather rare. In fact, this issue is quite relevant to the gelation mechanism. Information obtained in this direction will not only be quite helpful in understanding the events occurring in the initial gelation stage, but surely will shed some light on what takes place in the middle and later stages.

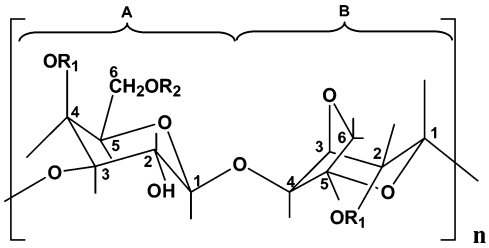

Figure 1. Idealized AB repeat unit of agarose polymer:[2] (A) 1,3 linked β-D-galactose residue; (B) 1,4 linked 3,6-anhydro-α-L-galactose residue. Native agarose: $R_1 = R_2 = R_3 = H$. Agarose sulfate: $R_1 = H$, $R_2 = SO_3^-$, $R_3 = 80\%\ H + 20\%\ SO_3^-$.

The purpose of this paper is to revisit the agarose gelation mechanism with emphasis on the topology evolution of the agarose gel using an in situ network detection method. Electrophoretic mobility measurements are performed to verify the results of the in situ network detection method. Rheological measurements are used to identify the induction time for the nucleation process. These findings suggest that the gelation process can be divided into three distinct stages—induction stage, gelation stage, and pseudoequilibrium stage—which are described by a schematic representation.

* To whom correspondence should be addressed. E-mail: phyliuxy@nus.edu.sg.

[†] Department of Chemical and Biomolecular Engineering, National University of Singapore.

[‡] Department of Physics, National University of Singapore.

[§] Hwa Chong Junior College.

10.1021/jp044473u CCC: $30.25
Published on Web 03/04/2005

Experimental Section

Materials and Gel Preparation. The agarose used in this experiment was SeaKem LE Agarose (high-melt, gelling temperature for 1.5% w/v 34.5−37.5 °C) and Bio-Rad Certified low-melt agarose. Agarose solutions were prepared by dispersing agarose powder in deionized water at room temperature at various concentrations (0.5% w/v to 3.0% w/v). To ensure the complete dissolution of agarose into deionized water, solutions were made by heating mixtures in a pressure vessel to 110 °C for high-melt (HM) agarose and 90 °C for low-melt (LM) agarose for 1 h. The hot solutions (so-called "sol") were then loaded carefully into cuvettes of a Cary 50 UV-Vis spectrophotometer for in situ network detection or transferred between the measuring plates of an advanced rheological expansion system (ARES-LS, Rheometric Scientific) for rheological studies. The quench rate was determined by inserting a thermocouple in the solution loaded in the cuvette for absorbance measurements. For rheological measurements the quench rate could be programmed using the temperature controller employing the Peltier effect.

In Situ Network Detection. *Correlation Length of Gel Network.* Network topology can be characterized by a correlation length ξ, which is the average distance between entanglements or the pore size. ξ can be obtained by both angular dependent light scattering[3] and turbidity spectrum.[9] For the former method, traditional design of the light scattering setup requires the kinetics to be sufficiently slow to allow for motor rotations and photon counting of the scattered light. Compared with the angular scanning method, obtaining the turbidity spectrum in the wavelength range of $\lambda = 700$ nm to 800 nm with a medium scanning rate needs only 10 s. Such a method was therefore chosen to probe gel topology evolution, based on that outlined by Aymard et al.[9] Turbidity can be calculated as $\tau(\lambda) = 2.3A(\lambda)/L$, where A is the absorbance and L is the optical path length. The turbidity of a solution of monodisperse optically isotropic particles is given by

$$\tau(\lambda) = H(\lambda)\cdot Q(\lambda)\cdot S(\lambda)\cdot M\cdot c \tag{1}$$

where M is the molecular weight (in g mol^{-1}), c is the particle concentration (in g cm^{-3}), H is the "optical constant function", S is the "interparticle correlation function", and Q is the "intraparticle dissipation factor", the integral form of form factor $P(\theta)$ over the range of scattering angles θ ranging from α to π, where α is the acceptance angle ($\sim$3°). In dilute conditions, $S = 1$.

$$H(\lambda) = \frac{32\pi^3 n_0^{\,2}(\mathrm{d}n/\mathrm{d}c)^2}{3N_A\lambda^4} \tag{2}$$

with n_0, dn/dc, and N_A being respectively the refractive index of the solvent, the refractive index increment of the particles with concentration, and the Avogadro number.

$$Q = \frac{3}{8}\int_\alpha^\pi P(\theta)\cdot(1+\cos^2\theta)\cdot\sin\theta\,\mathrm{d}\theta \tag{3}$$

The form factor of entangled Gaussian coils is given by

$$P(q) = \frac{1}{1+q^2\cdot\xi^2} \tag{4}$$

with the scattering wave vector, $q = 4\pi n_0 \sin(\theta/2)\lambda^{-1}$. Equation 1 can be simplified to

$$\mathrm{WLE} = \frac{\mathrm{d}\log\tau(\lambda)}{\mathrm{d}\log(\lambda)} = -4 + \alpha_1 + \alpha_2 + \frac{\mathrm{d}\log Q(\lambda)}{\mathrm{d}\log(\lambda)} \tag{5}$$

where

$$\alpha_1 = 2\frac{\mathrm{d}\log(n_0)}{\mathrm{d}\log(\lambda)} \tag{6}$$

$$\alpha_2 = 2\frac{\mathrm{d}\log(\mathrm{d}n/\mathrm{d}c)}{\mathrm{d}\log(\lambda)} \tag{7}$$

The first three terms on the right-hand side of eq 5 are derived from the wavelength dependence of the optical function $H(\lambda)$. For agarose,[9] $\alpha_1 = -0.0248$. For different temperatures, α_2 can be obtained from the study of Podesva et al.[10] on the variation of dn/dc of agarose with wavelength and temperature. Using eqs 3 and 4, the derivative of log Q with respect to log λ can be calculated and the wavelength exponent, WLE, can be determined for different ξ values. For ξ values of 1 to 30 nm and 2 to 100 μm, WLE shows marginal variation with ξ thereby introducing larger error in the estimation of pore size. In the intermediate range, the measurement of WLE provides a fast and noninvasive estimation of the pore size of the agarose gel.

Mass/Length Ratio and Radii of the Fiber Bundle Constituting the Gel Network. Modeling the gel network to be composed of cylindrical bundles of agarose chains, the turbidity τ can be expressed as a function of μ, the mass per unit length of the fibers in the bundle and its cross sectional radius, r.[11]

$$1/\tau\lambda^3 = (A/c)\mu^{-1} + (B/c)(r^2/\mu)\lambda^{-2} \tag{8}$$

where

$$A = \left[\frac{88}{15}\pi^3 n_0(\mathrm{d}n/\mathrm{d}c)^2/N_A\right]^{-1}; \qquad B = (92\pi^2 n_0^{\,2}/77)A \tag{9}$$

Equation 8 implies that a plot of $1/\tau\lambda^3$ vs λ^{-2} should give a straight line whose intercept is proportional to μ^{-1} while the ratio of slope to intercept is proportional to the square of the radius of the bundle. The turbidity data in the wavelength range 700 to 800 nm were used to determine μ and r.

Electrophoretic Mobility Measurements. The simplicity of the turbidity measurements described above is associated with the assumptions that the aqueous gelling system is composed of monodisperse optically isotropic particles and the system is dilute enough that the interparticle correlation function S(λ) in eq 1 can be treated as unity. However, the real gelling system may not satisfy these assumptions. As the pore size of agarose gel can also be determined through electrophoretic mobility measurements, these were used to check the validity of the in situ network detection method using turbidity. HM agarose solutions of concentrations 0.5, 1.0, and 1.5% w/v were prepared by adding agarose powder into 1X TBE buffer solution. Higher concentrations were not chosen as the resolution of the separation of the DNA molecules would be poor and require very long duration of electrophoresis. Evaporation of water due to boiling was taken into account in the dilution. The mixture was microwaved for 1 min and cooled until approximately 60 °C. Ethidium bromide (2.5 μL) was added to the mixture and the mixture was poured carefully into the gel-casting tray and left to stand for 20 min. Bio-Rad EZ Load 1 kB molecular ruler was then loaded into the wells. Electrophoresis was carried out for varying electric fields in the range 0.7 to 5 V/cm and suitable

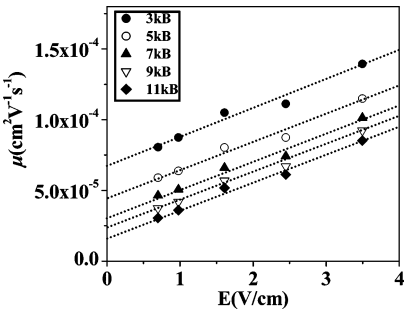

Figure 2. Electrophoretic mobility as a function of electric field in 0.5% agarose gel.

durations to get good separation of the DNA bands. The gel was illuminated by UV light and using AlphaDigiDoc software the image was analyzed to find the distance traveled by selected DNA molecules. Electrophoretic mobility μ can be obtained by measuring the distance traveled by various DNA segments for different duration and voltage. The electric field, E, applied should be sufficiently small. Plotting μ against E, the value of $\mu_{E\to 0}$ can be obtained (Figure 2).

Assuming that the DNA molecules reptate through the gel pores, the electrophoretic mobility is given by[12]

$$\mu_{E\to 0} = \mu_0\left(\frac{1}{3N}\right) \tag{10}$$

where μ_0 is the intrinsic mobility of DNA in TBE buffer solution[13] given by 4.3×10^{-4} cm^2 V^{-1} s^{-1}. A DNA chain of M base pair length is modeled as a Gaussian chain with a persistence length P, which is typically 50 nm.[14] Assuming Gaussian statistics,

$$\langle h^2\rangle = Na^2 = N_0(2P)^2 = L(2P) \tag{11}$$

Here $\langle h^2\rangle$ is the mean square end-to-end distance, equivalent to N blobs of mean square end-to-end distance a^2, where a is the tube diameter. N_0 is the number of Kuhn segments of the chain with length $2P$ and L is the contour length. $L = N_0(2P) = Mb$, with $b = 0.34$ nm being the inter-base pair distance along the DNA helix. From eqs 10 and 11,

$$a = \sqrt{Mb(2P)\frac{3\mu_{E\to 0}}{\mu_0}} \tag{12}$$

Hence, the pore diameter a can be calculated if $\mu_{E\to 0}$ is experimentally determined. $\mu_{E\to 0}$ is found by plotting values of μ for low values of electric field and extrapolating to zero electric field. This theory is valid only if the DNA molecules are larger than the gel pores, i.e., $N \gg 1$. Hence DNA fragments of large size have to be used. The mobility of large DNA molecules being very low, the duration of electrophoresis is typically several hours.

Rheological Measurements. The rheological properties of the agarose gelling system were measured using an advanced rheological expansion system (ARES, Rheometric Scientific). This system has already been used to gain many insights into the architecture of three-dimensional nanocrystal fiber networks through gelation of a small molecule gelator.[15] In the present study, the thermal sequence was strictly programmed so as to ensure that the samples experience the same thermal history as those in the absorbance measurements. The sample was subjected to sinusoidal oscillations by loading it between circular plates of diameter 25 mm, the gap between the two plates being 1 mm. The frequency was set to 1 Hz and the amplitude of the oscillations was controlled to obtain a 0.1% strain in the sample. Under this strain limit, the structure of the agarose gel is not destroyed by the measurements. Samples were covered with mineral oil to prevent evaporation during the measurements.

Results and Discussion

Kinetics of Agarose Gelation. Typical gelation kinetics is shown in Figure 3. HM agarose sol (0.5% w/v) was quenched to 21 °C at the cooling rate indicated in Figure 3a. Three stages (designated as I, II, and III in the figure) can be clearly identified. In stage I when the temperature is higher than 37 °C, the aqueous system remains in the sol state. Absorbance is very low and no aggregation is detectable. In this stage, the wavelength exponent (WLE), calculated from the absorbance readings (eq 5), changes randomly with time and therefore is not shown in Figure 3b. As temperature is further reduced (Stage II), absorbance, WLE, and hence the correlation length increase steeply with time and after $t = 20$ min the growth becomes gradual. This result indicates that agarose gelation starts from a nascent network formed when the Brownian diffusion of the chains slows down due to cooling below 35 °C. The entanglement points of the network act as nuclei for further assembly of the fibers. As more agarose fibers leave the sol state and join the assembly, the turbidity increases fast. This can be interpreted from the rapid increase of the correlation length (pore size for trapped solvent) and mass/length ratio of the fibers in the assembly as indicated in Figure 3, parts b and c. Meaningful data for these two parameters are available for $t > 10$ min. From Figure 3c, fiber radii do not change much as the mass/length ratio increases with time. This implies that fiber assembly in the early stage of gelation is quite loose and becomes more and more tightly packed due to the aggregation of the fibers upon gelation. Such an aggregation will first slow and finally stop because further aggregation requires the dissociation of existing junctions whereas the dissociation energy barrier is very high. This is shown in stage III. In this stage, the increase of all the parameters has slowed to become very gradual. WLE and correlation length have leveled off while the absorbance still increases with time. It appears that this stage concerns the refining of the network (for example, association of the dangling agarose chains to the fibrous network). The increase of the absorbance should mainly be due to the slight thickening of the network fibers.

Gelation kinetics was also studied using rheology, in which the temperature course was programmed in advance to strictly follow the temperature course shown in Figure 3a. The result is shown in Figure 3d and gelation rate can be characterized by the time rate of variation of storage modulus, G', given by dG'/dt. In the initial sol state, G' is extremely low. When gelation starts, fiber junctions appear and serve as the permanent nodes of the network. This causes G' to rise steeply with time. The time rate of variation of dG'/dt shown in Figure 3d indicates that gelation in the time duration corresponding to stage II is very fast. However, the pseudoequilibrium state extends over an extremely long time.

Identification of Gelation Mechanism. Now it is commonly accepted that agarose gelation occurs through a liquid−liquid-phase separation.[3−5,7] However, there still remains a matter of controversy about what its mechanism may be: spinodal decomposition (SD) or nucleation and growth (NG). Most researchers infer the underlying mechanism using static light scattering techniques (SLS).[3−5] For example, Manno et al.[3]

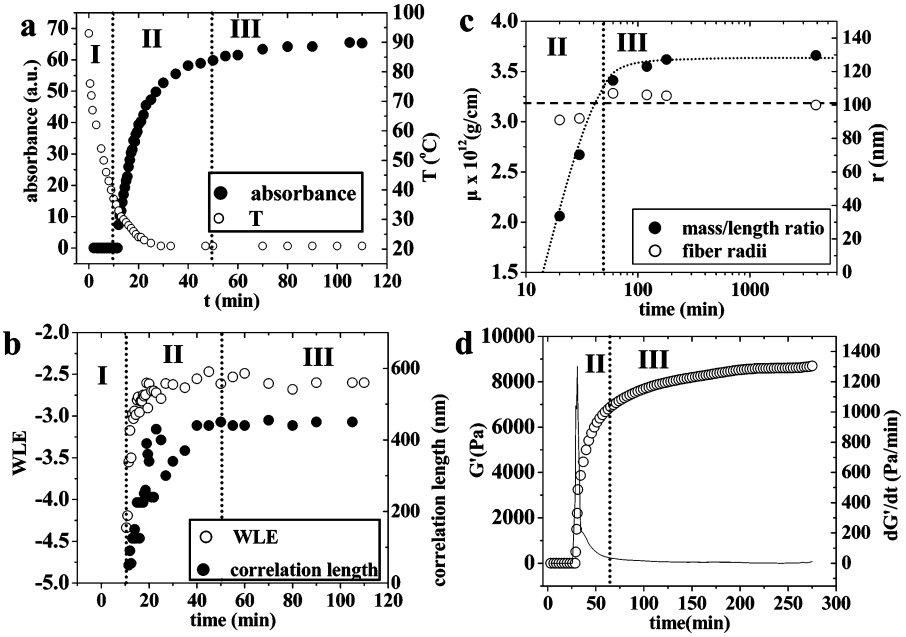

Figure 3. Gelation kinetics of HM agarose solution (0.5% w/v, quench to 21 °C, natural cooling).

consider spinodal decomposition, conformational change, and cross-linking as the three factors whose kinetic competition plays a central role in determining the final gel topology. In a 2% agarose solution, upon quenching to relatively high setting temperature (46.5 °C) spinodal decomposition occurs first and subsequent helix transition and cross-linking are promoted in the polymer-rich phase. Upon quenching to relatively low setting temperature (31 °C), helix transition is the fastest process and demixing is kinetically inhibited by cross-linking from the very beginning. However, these conclusions are somewhat contradictory to those obtained by Feke and Prins.[4] They found that for a 1% agarose solution, at low quenching temperature (25.5 °C), light scattering intensity distribution supports the spinodal decomposition process while at high quenching temperature (41 °C) above the spinodal temperature, the nucleated process would be more reasonable. Matsuo et al.[5] studied agarose solutions of concentrations of 1% to 2.5%, which upon quenching to 25 °C to 45 °C suggest the initial stage of gelation to be spinodal decomposition. The existence of at least three different versions of spinodal decomposition implies that the gelation mechanism needs to be reevaluated. As suggested by Guenet,[7] the occurrence of correlation peak and the time evolution of scattered intensity at low angle alone cannot give a conclusive proof of spinodal decomposition.

Dynamic light scattering (DLS) is also used to study the sol−gel transition in several systems such as associating polymer solutions,[16] polymer cluster solutions,[17] and thermoreversible gelling solutions.[18−23] The normalized intensity autocorrelation function of the scattered light is measured and is used to calculate the normalized time correlation function of the scattered elastic field, $g^1(q,t)$, which is identified with the dynamic structure factor $S(q,t)$. In the sol-state, $S(q,t)$ is single exponential and the relaxation rate is related to the cooperative diffusion coefficient, D_c. As sol−gel transition proceeds in the system, the decay of $S(q,t)$ is more complicated with an initial exponential decay followed by a stretched exponential. The characteristic time of the stretched exponential diverges to infinity as the system set to a gel. Polystyrene latex particles are also used as probe particles to follow the evolution of diffusion coefficient during sol−gel transition and the microscopic viscosity in the environment of the probe particle is used to characterize the sol−gel transition. However, following the kinetics of gelation using DLS is complicated by multiple scattering and also large fluctuations in intensity and relaxation time due to the onset of the gel network.[3b]

In this study we use a different approach to identify the gelation mechanism. A crucial difference between SD and NG is the existence of an induction time before the occurrence of the phase separation. If phase separation takes place through a nucleation and growth mechanism, an induction time should not only exist but also conform to the rules of the nucleation theory. This criterion is applicable for most NG predominant processes[24] including the gelation of organogels.[15]

As shown in Figure 3a, the quench rate is not constant and it becomes lower and lower when the sample temperature approaches the quench bath temperature. In such a case, gelation already occurs before the system approaches the final setting temperature. To clarify whether there really exists an induction time before phase separation, the same system was studied by ARES using a modified quench scheme. Employing the Peltier effect, ARES can achieve a constant quench rate as large as 30 deg C/min. Meanwhile, ARES can detect the response of the sample under a very small strain (0.1%) so that the gel structure will not be destroyed during the measurements. Therefore ARES is the ideal equipment for checking the existence of the induction time. To explore this aspect of gelation mechanism, 0.5% w/v HM agarose gel was first heated to 90 °C (well above T_{eq}, the melting temperature) to ensure that the gel was completely melted. The sol was then quenched at a cooling rate of 30 deg C/min to different final setting temperatures (21 to 27 °C). The storage modulus was monitored along with the temperature ramp to measure the induction time.

As shown in Figure 4a, the induction time t_i can be clearly detected when the quench rate is maintained as large as 30 deg C/min. According to 3D nucleation models, the nucleation rate J, the number of critical nuclei generated per unit time−volume, can be expressed as[25,26]

$$J = B \exp\left(-\frac{16\pi\gamma_{cf}^{3}\Omega^2}{3(kT)^3[\Delta\mu/kT]^2}f\right) \qquad (13)$$

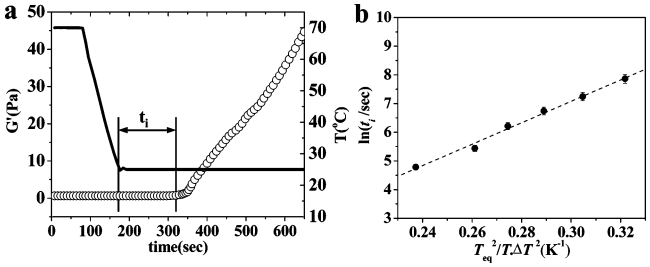

Figure 4. (a) Gelation kinetics of HM agarose solution (0.5% w/v, quench to 21 °C at 30 deg C/min). (b) The plot of $\ln(t_i) \sim T_{eq}^2/T\cdot\Delta T^2$. The dotted line is the linear fit.

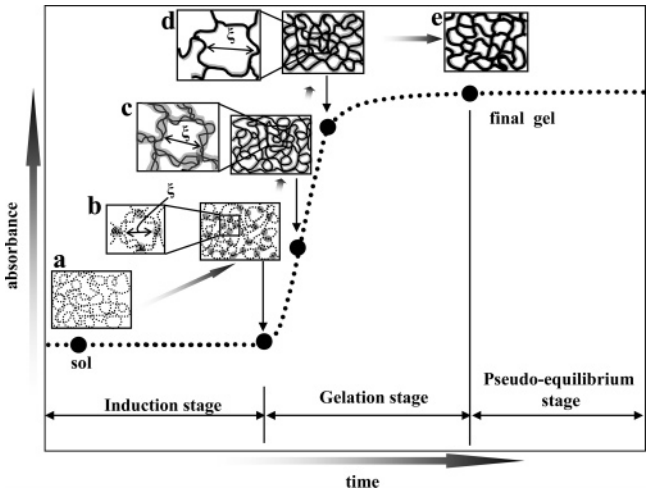

Figure 5. Schematic representation of agarose gelation.

with

$$\frac{\Delta\mu}{kT} \cong \frac{\Delta H_{diss}}{kT_{eq}T}\Delta T; \qquad \Delta T = T_{eq} - T \tag{14}$$

where k denotes Boltzmann's constant, T is temperature, Ω is the volume of growth units, B is a constant for a given system, f is the factor describing the structural correlation between foreign bodies and the nucleating phase,[25] ΔH_{diss} denotes the molar dissolution enthalpy of the nucleating phase, T_{eq} is the melting point for the 0.5% w/v HM agarose gel (~334.2 K according to our measurements), and T is the final setting temperature. If agarose gelation is initiated through the nucleation and growth mechanism,[26] one should have $t_i \sim 1/J$ and according to eq 13, we should have a linear relationship with $\ln(t_i) \sim 1/(kT)^3(\Delta\mu/kT)^2$. Using eq 14, we should have $\ln(t_i)$ proportional to $T_{eq}^2/T\cdot\Delta T^2$. As shown in Figure 4b, we indeed obtain such a linear relationship in agreement with similar results for organogels (vide Figure 3 of ref 15b). This result supports that the formation of the HM agarose gel is initiated through a nucleation and growth process.

Based on the above discussions, we may reinterpret the gelation kinetics in terms of liquid−liquid phase separation as indicated schematically in Figure 5. Upon quenching, agarose gelation is initiated through a nucleation and growth mechanism, leading to many nuclei composed of polymer-rich phases dispersed in the sol (state b in Figure 5). In this case, the correlation length is assigned to the average distance between the neighboring nuclei.[27] As the gelation progresses, the nuclei tend to grow and form a network of polymer-rich phases. The polymer-rich phases tend to coagulate so as to minimize the interface between the polymer-rich phase and polymer-poor phase in order to reduce the interfacial free energy. However,

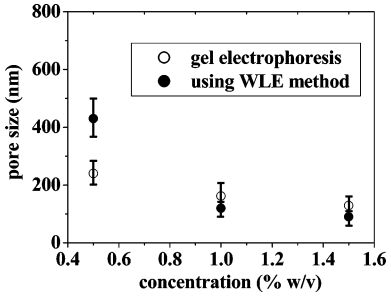

Figure 6. Comparison of results obtained by the WLE method and electrophoresis. The size of the error bar corresponds to the largest deviation from the mean of the measurements.

TABLE 1: Results for Gel Electrophoresis

concn/ %	base pairs/ kB	mobility $\mu_{E\to 0}$/ $\times 10^{-5}$ cm^2 V^{-1} s^{-1}	pore size a/ nm	mean a /nm
0.5	3	6.79	220	
	5	4.56	233	
	7	3.27	233	
	9	2.38	226	
	11	1.80	217	226
1.0	3	3.96	168	
	4	2.88	165	
	5	2.23	163	
	6	1.63	152	162
1.5	2	3.84	135	
	3	2.43	132	
	4	1.69	127	
	5	1.25	122	129

inhibited by the rigidity of the agarose chains[28,29] and due to the aggregation of these chains within the polymer-rich phase, large scale coagulation is unlikely to occur. Hence polymer-rich phases locally merge leading to a continuously increasing correlation length, in other words, pore size increases with time. In the initial stage of the gelation (stage b → c → d, Figure 5), the local coagulation of the polymer-rich phase readily occurs, causing the WLE and hence the correlation length to increase steeply with time (Figure 3b). However, in the later stage of gelation (stage d → e, Figure 5), most agarose chains are immobilized in the fiberous junctions and local coagulation becomes rather difficult. In this situation, aggregation of surrounding agarose chains from the polymer-poor phase to the fiberous framework leads to gradually increasing absorbance (Figure 3a) and G' (Figure 3d) while the correlation length remains almost constant (Figure 3b). To summarize, the agarose gelation is initiated by a nucleation and growth mechanism. Kinetics of the gelation is determined by the formation of nuclei of the polymer-rich phases, growth of the nuclei forming a network of polymer-rich phases, aggregation of agarose chains within the polymer-rich phase, and the local coagulation of the polymer-rich phases tending to approach the global minimum of the free energy of the whole system.

Electrophoretic Mobility Measurements. The validity of the determination of the pore size by turbidity measurements was verified by using electrophoresis. The pore sizes calculated using WLE are for the gels equilibrated for 24 h. Table 1 shows the results for gel electrophoresis. Figure 6 compares the pore sizes obtained from WLE and gel electrophoresis methods. Both methods show a distinct trend of decreasing pore size with increasing concentration. This result shows that both methods are valid to determine agarose pore sizes and distinct trend related to them. The disparity in pore size obtained by the two methods may be attributed to the difference in the preparation method of agarose gel and lack of temperature stabilization in electrophoresis over several hours. Another problem with the

gel electrophoresis method is the difficulty in obtaining vanishing electric fields. The inaccuracy may be accounted for by the fact that the $\mu_{E\to 0}$ values are estimated from a linear plot for significant electric fields. Also any variations in the parameters assumed such as free solution mobility, μ_0, and persistence length, P, will significantly affect the calculated value of pore size (eq 12). Compared to electrophoresis, the WLE method enables measurement of pore size in a wide range of concentration and temperature which are of general interest in various applications. It is also a fast and noninvasive method where the gel structure is the least affected by the experimental tools.

Conclusions

Kinetics and the evolution of the agarose gel topology are discussed in this study. Using aqueous high-melting (HM) agarose solution (0.5% w/v) as the model system, we find that the gelation process can be clearly divided into three stages: induction stage, gelation stage, and pseudoequilibrium stage. Gelation mechanism has been investigated using rheological measurements. When a quench rate as large as 30 deg C/min is employed, the induction time for the nucleation process can be distinctly identified even when the sample is quenched to very low temperatures (e.g. 21 °C). The linear relationship between $\ln(t_i)$ and $1/(kT)^3(\Delta\mu/kT)^2$ supports that the agarose gelation is initiated through a nucleation and growth mechanism. A schematic representation of the three stages of the gelation process is given. Aggregation of agarose chains promoted in the polymer rich-phase is evident from the increasing mass/length ratio of the fiber bundles. Continuously increasing correlation length (pore size) may be attributed to the coagulation of the local polymer-rich phases so as to approach the global minimum of the free energy of the gelling system. Finally, measurement of the correlation length by the WLE method is verified by gel electrophoresis.

Acknowledgment. The authors gratefully acknowledge the financial support from the National University of Singapore (grant number R-279-000-108-112) and A*star (project No. 0221010036). Part of this work was performed under Science Research Programme (SRP) 2004-2005 of the National University of Singapore. The authors thank Mr. T. K. S. Jonathan for his help in kinetics study and Dr. Rongyao Wang and Dr. Jingliang Li for many fruitful discussions.

References and Notes

(1) (a) Rees, D. A. *Biochem. J.* **1972**, *126*, 257. (b) Dea, I. C. M.; McKinnon, A. A.; Rees, D. A. *J. Mol. Biol.* **1972**, *68*, 153. (c) Arnott, S.; Fulmer, A.; Scott, W. E.; Dea, I. C. M.; Moorhouse, R.; Rees, D. A. *J. Mol. Biol.* **1974**, *90*, 269.

(2) *Thermoreversible networks*: *viscoelastic properties and structure of gels*; Nijenhuis, K. te., Ed.; Springer-Verlag: Berlin, Germany, 1997.

(3) (a) Manno, M.; Emanuele, A.; Martorana, V.; Bulone, D.; San Biagio, P. L.; Palma-Vittorelli, M. B.; Palma, M. U. *Phys. Rev. E* **1999**, *59*, 2222. (b) Bulone, D.; Giacomazza, D.; Martorana, V.; Newman, J.; San Biagio, P. L. *Phys. Rev. E* **2004**, *69*, 041401−1.

(4) Feke, G. T.; Prins, W. *Macromolecules* **1974**, *7*, 527.

(5) Matsuo, M.; Tanaka, T.; Ma, L. *Polymer* **2002**, *43*, 5299.

(6) Cahn, J. W. *J. Chem. Phys.* **1965**, *42*, 93.

(7) *Thermoreversible Gelation of Polymers and biopolymers*; Guenet, J.-M., Ed.; Academic Press: London, UK, 1992

(8) Watase, M.; Nishinari, K. *Polym. J.* **1986**, *18*, 1017.

(9) Aymard, P.; Martin, D. R.; Plucknett, K.; Foster, T. J.; Clark, A. H.; Norton, I. T. *Biopolymers* **2001**, *59*, 131.

(10) Podesva, J.; Prochazka, O.; Medin, A. *Polymer* **1995**, *36*, 4967.

(11) Carr, M. E.; Gabriel, D. A. *Macromolecules* **1980**, *13*, 1473.

(12) Tinland, B.; Pernodet, N.; Weill, G. *Electrophoresis* **1996**, *17*, 1046.

(13) Strutz, K.; Stellwagen, N. C. *Electrophoresis* **1998**, *19*, 635.

(14) Lu, Y.; Weers, B.; Stellwagen, N. C. *Biopolymers* **2002**, *61*, 261.

(15) (a) Liu, X. Y.; Sawant, P. D.; Tan, W. B.; Noor, I. B. M.; Pramesti, C.; Chen, B. H. *J. Am. Chem. Soc.* **2002**, *124*, 15055. (b) Liu, X. Y.; Sawant, P. D. *Adv. Mater.* **2002**, *14*, 421.

(16) Nystrom, B.; Walderhaug, H.; Hansen, F. K. *J. Phys. Chem.* **1993**, *97*, 7743.

(17) Adam, M.; Delsanti, M.; Munch, J. P.; Durand, D. *Phys. Rev. Lett.* **1988**, *61*, 706.

(18) Narayanan, J.; Deotare, V. W.; Bandyopadhyay, R.; Sood, A. K. *J. Colloid Interface Sci.* **2002**, *245*, 267.

(19) Martin, J. E.; Wilcoxon, J. P. *Phys. Rev. Lett.* **1988**, *61*, 373.

(20) Martin, J. E.; Wilcoxon, J. P.; Odinek, J. *Phys. Rev. A* **1991**, *43*, 858.

(21) Ren, S. Z.; Shi, W. F.; Zhang, W. B.; Sorensen, C. M. *Phys. Rev. A* **1992**, *45*, 2416.

(22) Bauer, J.; Burchard, W. J. *J. Phys. II France* **1992**, *2*, 1053.

(23) Maity, S.; Bohidar, H. B. *Phys. Rev. E* **1998**, *58*, 729.

(24) (a) Liu, X. Y. *J. Chem. Phys.* **1999**, *111*, 1628 (b) Liu, X. Y. *Appl. Phys. Lett.* **2001**, *79*, 3603. (c) Liu, X. Y.; Du, N. *J. Biol. Chem.* **2004**, *279*, 6124.

(25) (a) *Modern Crystallography III Crystal Growth*; Chernov, A. A., Ed.; Springer-Verlag: Berlin, Germany, 1984. (b) Liu, X. Y.; Maiwa, K.; Tsukamoto, K. *J. Chem. Phys.* **1997**, *106*, 1870.

(26) (a) Liu, X. Y. *J. Chem. Phys.* **2000**, *112*, 9949. (b) Liu, X. Y. In *Advances in Crystal Growth Research*; Sato, K., Nakajima, K., Furukawa, Y., Eds.; Elsevier: Amsterdam, The Netherlands, 2001.

(27) Kanaya, T.; Ohkura, M.; Kaji, K.; Furusaka, M.; Misawa, M. *Macromolecules* **1994**, *27*, 5609.

(28) Ramzi, M.; Rochas, C.; Guenet, J.-M. *Macromolecules* **1998**, *31*, 6106.

(29) Clark A. H. In *Gums and Stabilisers for the Food Industry 10*; Williams, P. A., Phillips G. O., Eds.; Royal Society of Chemistry: Cambridge, UK, 2000.